

Catalysis Science & Technology

Accepted Manuscript



This is an *Accepted Manuscript*, which has been through the Royal Society of Chemistry peer review process and has been accepted for publication.

Accepted Manuscripts are published online shortly after acceptance, before technical editing, formatting and proof reading. Using this free service, authors can make their results available to the community, in citable form, before we publish the edited article. We will replace this *Accepted Manuscript* with the edited and formatted *Advance Article* as soon as it is available.

You can find more information about *Accepted Manuscripts* in the [Information for Authors](#).

Please note that technical editing may introduce minor changes to the text and/or graphics, which may alter content. The journal's standard [Terms & Conditions](#) and the [Ethical guidelines](#) still apply. In no event shall the Royal Society of Chemistry be held responsible for any errors or omissions in this *Accepted Manuscript* or any consequences arising from the use of any information it contains.



Hierarchical ZSM-11 Zeolite Prepared by Alkaline Treatment with Mixed Solution of NaOH and CTAB: Characterization and Application for Alkylation of Benzene with Dimethyl Ether

Cite this: DOI 10.1039/x0xx00000x

Hui Liu,^{ab} Sujuan Xie,^a Wenjie Xin,^a Shenglin Liu^a and Longya Xu^{a*}

A facile alkaline treatment with surfactant cetyltrimethylammonium bromide (CTAB) addition was presented to prepare hierarchical ZSM-11 zeolite (Z-xat-yCTAB). The textural and structural properties of Z-xat-yCTAB were characterized by XRD, adsorption and desorption of N₂ and benzene. By virtue of CTAB addition, uniform intracrystalline mesopore distribution centered ca. 4.2 nm was introduced accompanied by well protected microporosity. Based on characterization results such as TEM images, BJH curves as well as ²⁹Si and ²⁷Al MAS NMR spectra, the composite effects of NaOH and CTAB on mesoporosity production were proposed. Acidity was characterized thoroughly by FTIR of adsorbed pyridine (Py-IR) and pivalonitrile. Accordingly, the ratio and accessibility factor of Brønsted and Lewis acid sites were discussed systematically. In the alkylation of benzene with dimethyl ether, Z-xat-yCTAB series samples exhibited better reaction stability than ZSM-11 sample treated with NaOH solution. The catalytic promotion could be attributed to the dual effects of NaOH and CTAB on the porosity and acidity regulation. Moreover, based on the correlation between the reaction stability and the ratio of Brønsted to Lewis acid concentration with weak-medium strength, measured by Py-IR, it was revealed that the acidity regulation should play a more important role for the better reaction stability. In addition, the physicochemical properties and reaction activity were compared between ZSM-11 samples derived from alkaline treatment with CTAB addition and with tetrapropylammonium bromide (TPABr) addition under the same conditions.

Received 00th January 20xx,
Accepted 00th January 20xx

DOI: 10.1039/x0xx00000x

www.rsc.org/

Introduction

The hierarchical zeolite materials have drawn plentiful attention in the field of porous materials, since they combine the advantage of microporous materials with mesoporous ones^{1,2}. They exhibit much better catalytic performance as compared to conventional microporous zeolites in a series of catalytic reactions³⁻⁵. Bottom-up and top-down approaches have been developed to prepare the hierarchical zeolites^{6,7}. The typical top-down approach of alkaline treatment by treating zeolites in an alkaline medium is thought to be the most effective alternative to introduce mesoporosity, in terms of simplicity, efficiency and economy.

Recently, zeolite treated with alkaline solution in the presence of long-chain alkylammonium surfactants⁸⁻¹⁶, such as cetyltrimethylammonium bromide (CTAB), has sparked a surge of interest. By this means, hierarchical zeolites with uniform mesopores and tuned acidity was obtained, which resolves the problems of broad mesopore distribution and relatively poor solid yield of that via pure NaOH treatment^{9,10,15,17}. In the case of ZSM-5 alkaline

treatment with CTAB addition, the development of mesoporosity and the parallel preservation of microporosity were ensured^{9,10}. To the best of our knowledge, how the NaOH and CTAB exactly affect the desilication to produce mesopores in the alkaline solution remains in its infancy, despite copious quantities of investigations about this issue¹⁸⁻²⁰. Besides, owing to the symmetrical and nonmicelle forming nature, the tetraalkylammonium cation such as tetrapropylammonium bromide (TPABr) can be added into alkaline solution to obtain hierarchical zeolites. J. Pérez-Ramírez et al.^{21,22} reported that USY and beta zeolites alkaline treated with NaOH and TPABr showed excellent alkylation performance.

The external acidity has been highlighted for hierarchical zeolites, especially by means of IR studies of lutidine and collidine^{23,24} and 2,6-di-tert-butylpyridine²⁵ adsorption. However, these studies were limited to Brønsted acid sites only. Alternately, the IR experiment of pivalonitrile adsorption at room temperature was used to characterize both Brønsted and Lewis acid sites situated on external surface and in pore mouths of hierarchical ZSM-5^{13,14,26} and beta²⁷ zeolites.

The alkylation of benzene with dimethyl ether (DME) has been evidenced a noteworthy and effective approach of benzene reduction and the aromatic hydrocarbon production^{28,29}. Besides, DME is a more active methylation agent compared with methanol. It was reported that DME is activated by the Brønsted acid sites of zeolites and adsorbed methoxy and methyl species are formed²⁹. Zn-ZSM-11 was found to exhibit significantly better catalytic performance compared to Zn-ZSM-5²⁸, although these two zeolites shared many

^a State Key Laboratory of Catalysis, Dalian Institute of Chemical Physics, Chinese Academy of Sciences, Dalian, 116023, China, Fax: (+86)411-84379279, E-mail: lyxu@dicp.ac.cn.

^b University of Chinese Academy of Sciences, Beijing, 100049, China.

Electronic Supplementary Information (ESI) available: See DOI:10.1039/x0xx00000x

similar structural features. In addition, a possible reaction route was suggested in our previous report over the ZSM-11 catalysts treated with pure NaOH³⁰.

Previously, the physicochemical properties and reaction performances of ZSM-11 samples treated by NaOH with different concentrations were investigated³⁰. Herein, ZSM-11 zeolite was studied systematically via NaOH treatment with CTAB addition. The effects of NaOH and CTAB on mesopores generation were discussed in detail, combined with BJH pore size distributions, transmission electron microscopy images and ²⁹Si and ²⁷Al MAS NMR results. The ratio of Brønsted to Lewis acid site of the total acidity and that located on the external surface of zeolite, and the corresponding accessibility factor¹³ detected by FTIR technique adsorbed of pyridine and pivalonitrile were investigated. Then, the alkylation of benzene with DME was used as a model reaction to evaluate the obtained hierarchical ZSM-11 zeolites. Accordingly, the differences in the reaction stability were investigated and relevant with the physicochemical properties of the prepared hierarchical ZSM-11. In addition, the physicochemical properties and reaction performances were compared between ZSM-11 catalysts obtained by CTAB assisted alkaline treatment and by TPABr assisted alkaline treatment.

Experimental Section

Catalyst preparation

ZSM-11 zeolite sample used in this work was synthesized in laboratory based on our previous work with a Si/Al₂ ratio of 53 and particle size ranging in 300–400 nm³¹. The template was first removed by calcinations of the material at 540 °C for 4 h in air. The as synthesized ZSM-11 was further desilicated by a mixed solution of NaOH and CTAB as the follows.

In one series, the calcined ZSM-11 zeolite powder of 8 g was then treated in a series of aqueous NaOH solutions with the concentration ranging from 0.1 to 0.6 M and the concentration of CTAB fixed at 0.05 M of 280 ml under stirring at 75 °C for 15 min. In the other series, the sample was treated with the aqueous NaOH solution fixed at 0.5 M, but the concentration of CTAB ranging from 0.01 to 0.1 M of 280 ml under stirring at 75 °C for 15 min. The suspensions were quenched in cold water and filtered, and the solids were washed to be neutral with deionized water. Subsequently, the samples were dried and calcined at 550 °C for 6 h to remove the residual CTAB. Then, all the samples were converted to the protonic form by conventional ion exchange in aqueous NH₄NO₃ solution (0.8 M, 80 °C, 1 h, 20 cm³ per gram of zeolite for 3 times), followed by calcination (air condition, 510 °C, 3 h). The obtained samples were denoted as Z-*x*at-0.05CTAB and Z-0.5at-*y*CTAB, where *x* and *y* presented the concentrations of NaOH and CTAB solution, respectively.

For comparison, both Z-0.5at and Z-0.05CTAB were also prepared. The former was treated with only a solution of 0.5 M NaOH and the latter with only 0.05 M CTAB. Furthermore, Z-*x*at-0.05TPABr (*x* = 0, 0.2, 0.28, 0.35 and 0.5) and Z-0.5at-0.1TPABr samples were prepared under the same conditions as that treated with NaOH and CTAB, respectively.

Catalyst characterization

X-ray diffraction (XRD) patterns were collected on an X'Pert PRO X-ray diffractometer using Cu K α radiation (40 kV, 40 mA), with a 2 θ scanning range from 5° to 50° at a scanning rate of 10°/min. The relative crystallinity (RC) was calculated based on the relative areas of the reflection at $2\theta = 7.9\pm 0.1^\circ$, $8.8\pm 0.1^\circ$, $23.0\pm 0.1^\circ$, $23.8\pm 0.1^\circ$ and $45.0\pm 0.1^\circ$ of the prepared samples with that of the pristine HZSM-11

(whose RC was assumed as 100 %). X-ray fluorescence (XRF) experiments were conducted on a Philips Magix 601X X-ray fluorescence spectrometer. Solid state ²⁹Si and ²⁷Al MAS NMR measurements were performed on a Bruker Avance III 500 MHz spectrometer. Prior to ²⁷Al MAS NMR measurements, all the samples were fully hydrated with NH₄NO₃ saturated solution in a closed container.

N₂ adsorption and desorption experiments were performed on Micromeritics ASAP-2020 system at liquid nitrogen temperature of -196 °C. Prior to analysis, each sample was degassed at 350 °C for 10 h. The Brunauer-Emmett-Teller (BET) equation was used to calculate the special surface area with the adsorption branch, while the *t*-plot method was used to estimate the micropore volume of zeolitic materials.

Scanning electron microscopy (SEM) was performed using a JSM-7800F field-emission microscope at an acceleration voltage of 30 kV. Transmission electron microscopy (TEM) images were obtained with a JEM-2100 microscope at an acceleration voltage of 200 kV. Prior to observation, the samples were dispersed in anhydrous alcohol using ultrasonic technique, and then the resultant suspension were dropwise added to a micro grid membrane and dried in air.

Pyridine adsorption-IR (Py-IR) was carried out on a Vertex 70 IR spectrometer at 4 cm⁻¹ resolution. The sample powder was pressed into a self-supported wafer (13 mm diameter) of ca. 10 mg, and then the wafer was placed in an in situ cell. The pretreatment of the fresh samples was conducted as follows. The cell containing a zeolite wafer was evacuated while slowly increasing the temperature from room temperature (r.t.) to 450 °C and was evacuated at 450 °C for 1 h. A spectrum was recorded as background after the wafer was cooled down to r.t.. Subsequently, the sample was saturated with pyridine vapor for 20 min at 0 °C and the excess of pyridine was removed under vacuum at 150 °C for 0.5 h. Finally, the IR spectrum of sample was collected at r.t. to quantify the total acidity. Then the excess of pyridine on the sample was further removed under vacuum at 450 °C for 0.5 h, after cooling to r.t., it was followed by IR measurements to quantify the strong acidity. The bands at ca. 1540 cm⁻¹ and ca. 1450 cm⁻¹ were integrated to determine the concentration of Brønsted and Lewis acid sites, respectively.

Pivalonitrile-adsorption IR (Pn-IR) was conducted on the same instrument as that of Py-IR. After pretreatment, the sample was saturated with pivalonitrile and the excess of pivalonitrile was removed under vacuum at r.t. for 0.5 h, and then it was followed by IR measurements to quantify the amount of acid sites located on external surface and in pore mouths of the zeolite samples. The ratio of Brønsted to Lewis acid concentration thus determined was denoted as B/L-*Pn*. The accessibility factor (AF) was defined as the ratio of concentration of Brønsted (AF_B) and Lewis (AF_L) acid sites able to interact with pivalonitrile to the total Brønsted and Lewis acid concentrations determined with pyridine adsorption, which was followed as Ref.¹³.

The benzene adsorption-desorption isotherms were performed on an intelligent gravimetric analyzer (IGA-100) from Hiden Isochema Ltd. In a typical run, 30 mg sample was loaded into the bag. Prior to the sorption measurements, sample was outgassed under pressure less than 10⁻³ Pa at 300 °C for 2 h. Adsorption-desorption isotherms were obtained at 40 °C with a water batch and the equilibrium pressures were determined by high-accuracy Baratron pressure transducers. The corresponding curve of mass changes during the uptake process was recorded.

Catalyst evaluation

The alkylation of benzene with DME was performed in a stainless fixed bed reactor. In a typical run, 1 g catalyst was located in the middle part of the reactor and pretreated at 500 °C for 1 h in N₂ flow.

Table 1 Textural and physiochemical data of ZSM-11 samples treated with NaOH and CTAB.

Samples	Treatment condition		Si/Al ₂ ^a	RC ^b	Yield (%)	Textural data			
	C _{NaOH} (molL ⁻¹)	C _{CTAB} (molL ⁻¹)				S _{BET} (m ² g ⁻¹)	S _{ext} (m ² g ⁻¹)	V _{micro} (cm ³ g ⁻¹)	V _{meso} (cm ³ g ⁻¹)
Z-0.5at	0.5	-	16	62	26	503	306	0.087	1.145
Z-0.5at-0.01CTAB	0.5	0.01	32	85	48	503	262	0.108	0.719
Z-0.5at-0.03CTAB	0.5	0.03	39	90	54	536	287	0.111	0.712
Z-0.5at-0.05CTAB	0.5	0.05	40	89	58	523	281	0.109	0.706
Z-0.5at-0.075CTAB	0.5	0.075	41	92	59	518	275	0.109	0.689
Z-0.5at-0.1CTAB	0.5	0.1	46	98	69	474	187	0.129	0.561
HZSM-11	-	-	53	100	-	371	112	0.117	0.300
Z-0.05CTAB	-	0.05	57	106	89	381	115	0.121	0.314
Z-0.1at-0.05CTAB	0.1	0.05	55	105	74	420	160	0.117	0.371
Z-0.3at-0.05CTAB	0.3	0.05	49	104	66	475	221	0.115	0.544
Z-0.6at-0.05CTAB	0.6	0.05	39	87	41	555	314	0.108	0.903

^a Si/Al₂: Molar ratio determined by XRF.^b RC (%): Relative crystallinity.

Unless specified, the reaction was performed under the conditions of 450 °C, 0.1 MPa, $n(\text{benzene})/n(\text{DME}) = 2$, and the DME weight hourly space velocity (WHSV) of 8 h⁻¹. Both gas and liquid products were collected and analyzed in a GC (Agilent 7890A) equipped with a FID, and a PONA capillary column (50 m×0.2 mm×0.5 μm).

Results and discussion

Textural and physiochemical characterization

Z-xat-yCTAB ($x = 0-0.6 \text{ molL}^{-1}$, $y = 0.01-0.1 \text{ molL}^{-1}$) series samples were characterized by XRD technique, and the corresponding relative crystallinity values (RC) as well as Si/Al₂ molar ratios were presented in Tables 1. No ordered mesopore was observed according to the low angle XRD patterns (not shown here). The wide angle XRD patterns (Fig. S1) showed that all Z-xat-yCTAB samples kept MEL structure. In comparison with the pristine HZSM-11, Si/Al₂ ratio and RC of Z-0.05CTAB slightly increased to 57 and 106 %, respectively. This could be ascribed to that CTAB could wash off some amorphous aluminum species on the zeolite crystal³². For Z-0.5at-yCTAB series samples, both the Si/Al₂ ratio and RC increased with the increasing CTAB concentration (denoted as C_{CTAB}). While the Si/Al₂ ratio of the samples were not affected by the C_{CTAB} in the case of ZSM-5 zeolite treated by NaOH and CTAB⁹. For Z-xat-0.05CTAB, Si/Al₂ ratio ranged from 55 to 39 and RC ranged from 105 % to 87 % with NaOH concentration (denoted as C_{NaOH}) increasing from 0.1 to 0.6 M. On the whole, both values of Z-xat-0.05CTAB were higher than those of ZSM-11 zeolites treated with pure NaOH (Z-xat)³⁰, which was similar to the case of ZSM-5^{8,9}, due to the protective effect of CTAB³³.

The solid yields of Z-xat-yCTAB samples were higher than that of Z-0.5at (26 %), and were in accord with previous reports.^{21,22} Generally, the solid yield increased with C_{CTAB} for Z-0.5at-yCTAB, which may benefit from protection of zeolite structure due to adsorption of CTAB on the external surface²². It decreased with C_{NaOH} for Z-xat-0.05CTAB, as the protection from CTAB was gradually no match for the corrosion from NaOH.

The N₂ adsorption and desorption isotherms (Fig. 1a) of Z-0.5at-yCTAB showed typical features of hierarchical zeolites, namely, the adsorption isotherms with a steep rise at P/P₀ < 0.01 representing micropores zeolites, and hysteresis loop at P/P₀ = 0.44-1, corresponding to the existence of dissimilar mesopores³². The shapes of these isotherms had no evident change with the increasing C_{CTAB}. While the adsorption and desorption isotherms of Z-0.5at

showed a steeper increase in the region of P/P₀ = 0.8-1 (Fig. S2), which was typical for intercrystalline mesopores.

In the cases of Z-xat-0.05CTAB (Fig. 1c), C_{NaOH} played a significant role in the physiochemical properties. Z-0.05CTAB and Z-0.1at-0.05CTAB showed a type I isotherm typical for micropore zeolites, similar to HZSM-11. Other samples exhibited prominent hysteresis loops at P/P₀ = 0.44-1. As for Z-0.6at-0.05CTAB, the major hysteresis loop occurred at P/P₀ > 0.6, representing greater mesopores.

The BJH curves for Z-0.5at-yCTAB samples were shown in Fig. 1b. In contrast to Z-0.5at with a broad pore size distribution (PSD) of 10-100 nm (Fig. S2), Z-0.5at-yCTAB zeolites exhibited a clear band centered at ca. 4.2 nm, different from the sharp band centered at 5-6 nm in the case of ZSM-5 zeolite⁹. This band intensity first increased and then decreased with the increase of C_{CTAB}. Therein, the samples Z-0.5at-yCTAB ($y = 0.3-0.075$) showed the highest intensity among the tested samples.

Fig. 1d presented the PSDs of Z-xat-0.05CTAB series samples. Z-0.05CTAB zeolite showed a very similar PSD with HZSM-11 and almost the same mesoporosity could be observed (0.314 and 0.300 cm³g⁻¹, respectively). There was also no clear band corresponding to mesoporosity in the case of Z-0.1at-0.05CTAB. As for Z-0.3at-0.05CTAB, a weak wide band centered at ca. 3 nm occurred. While for Z-xat-0.05CTAB samples with x higher than 0.3 the center of this band shifted to ca. 4.2 nm. Besides, the intensity of the band centered at ca. 4.2 nm reached the highest value for Z-0.5at-0.05CTAB and Z-0.6at-0.05CTAB. Especially, the Z-0.6at-0.05CTAB zeolite showed a bimodal pore distribution, with a more intense band centered at ca. 18 nm and a smaller one at ca. 4.2 nm.

The textural data were summarized in Tables 1. Z-xat-0.05CTAB samples showed lower external surface area (S_{ext}) and mesopore volume (V_{meso}) compared to Z-xat³⁰, indicating that surfactant of CTAB protected ZSM-11 zeolite from NaOH corrosion, which was significantly different from the case of ZSM-5 zeolite^{9,10}. The micropore volume (V_{micro}) of Z-0.5at-yCTAB maintained at 0.108-0.129 cm³g⁻¹ with C_{CTAB} varying from 0.01 to 0.1 M, meanwhile the V_{meso} first kept constant of ca. 0.710 cm³g⁻¹ and then slightly decreased to 0.561 cm³g⁻¹. Increasing the C_{NaOH}, the V_{micro} of Z-xat-0.05CTAB slightly decreased from 0.121 to 0.108 cm³g⁻¹, meanwhile the mesoporosity would increase clearly. Therein, Z-0.6at-0.05CTAB zeolite exhibited the highest S_{ext} of 314 m²g⁻¹ and V_{meso} of 0.90 cm³g⁻¹, respectively. In the cases of Z-xat³⁰, the V_{meso} was improved significantly at the expense of V_{micro}. These further verified the protective effect of CTAB.

The adsorption and desorption isotherms of benzene at 40 °C on the four typical samples were presented in Fig. 2. Both the benzene sorption isotherm of the HZSM-11 and the one of Z-0.05CTAB showed an approximate type I adsorption curve with a steep uptake

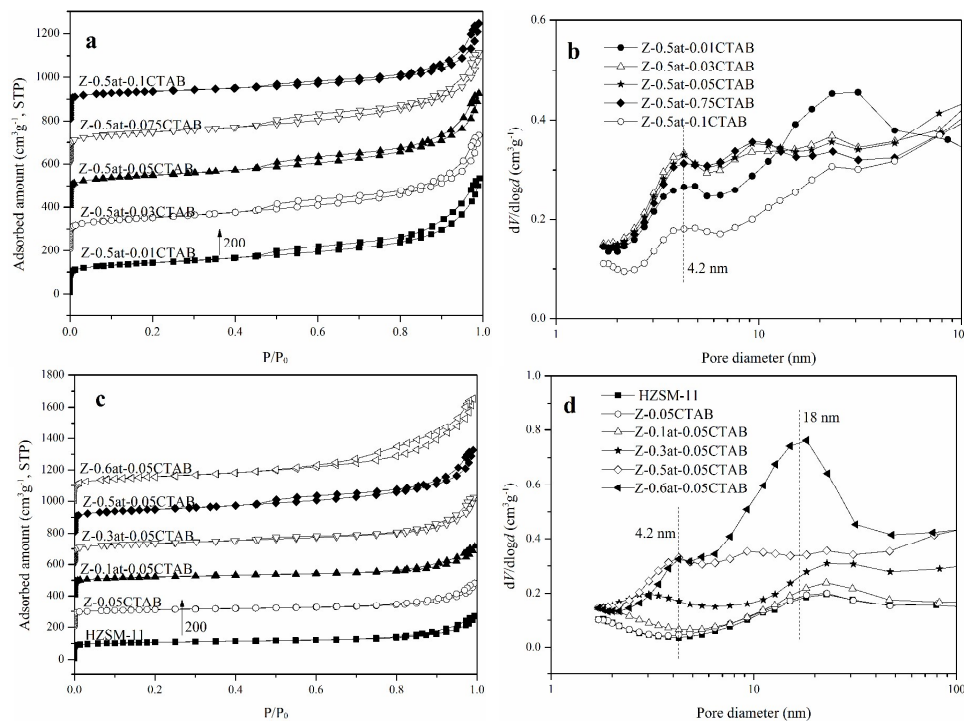


Fig. 1 Nitrogen adsorption and desorption isotherms at -196 °C (a, c); and BJH pore size distribution plots derived from the adsorption branch (b, d) for Z-xat-yCTAB.

at low relative pressure (P/P_0) from micropores and gradual uptake at high P/P_0 from intercrystalline voids, indicating that the adsorption behavior is predominated by micropores³⁴. For Z-0.5at and Z-0.5at-0.05CTAB, a more obviously enhanced adsorption phenomenon appeared even at high P/P_0 (≤ 0.9), implying the remarkable mesopore properties³⁴. The adsorption capacity for the tested samples followed the sequences of Z-0.5at > Z-0.5at-0.05CTAB > Z-0.05CTAB and HZSM-11, which was parallel with the variation

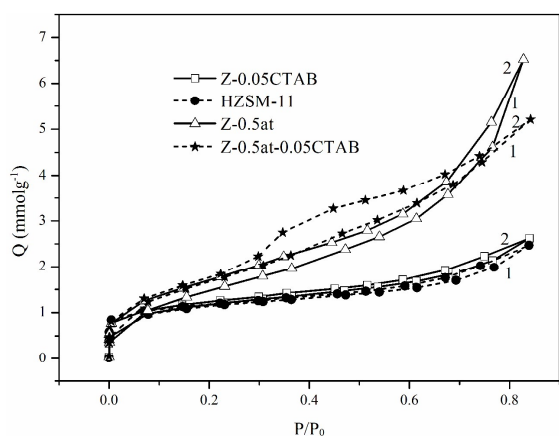


Fig. 2 Adsorption and desorption isotherms of benzene on different ZSM-11 samples measured by IGA at 40 °C (1-adsorption branch; 2-desorption branch).

trend of V_{meso} (Table 1).

To detect the coordination state of Al species in the samples, ²⁷Al MAS NMR measurements were done and the spectra were shown in Fig. 3. It is well known that the strong peak centered at ca. 57 ppm, can be attributed to the Al species tetrahedrally coordinated in the framework (Al_{fra}), and that the small peak centered at ca. 0 ppm, can be assigned to octahedrally coordinated extra-framework Al (Al_{ext})³⁰. Clearly, Z-0.5at-yCTAB series samples showed lower peak area of Al_{ext} than Z-0.5at, as dealumination of the zeolite framework was hindered due to the presence of CTAB during alkaline treatment²⁰, or the adsorption of CTAB on the zeolite largely inhibited surface realumination²¹. Meanwhile, this peak area for Z-0.5at-0.05CTAB series samples was higher compared with that for Z-0.05CTAB sample, since some Al_{fra} became Al_{ext}^{35,36} during alkaline treatment.

To further uncover the structural changes, the spectra of ²⁹Si MAS NMR for various samples were given in Fig. 4 and the corresponding results were listed in Table 2. The deconvolution of ²⁹Si MAS NMR spectra of all Z-xat-yCTAB samples presented three peaks centered at ca. -114 (Si(4Si)), -106 (Si(3Si, 1Al)), and -100 (SiOH) ppm^{37,38}, respectively. Due to the serious desilication by pure NaOH solution, Z-0.5at showed a significantly lower proportion of Si(4Si) and a higher proportion of Si(3Si, 1Al), and the peak of SiOH slightly shifted to -97 ppm, indicating the selective leaching of Si which was not surrounded by Al was confirmed during alkaline treatment³⁹. Compared to Z-0.5at, CTAB addition clearly increased the proportion of Si(4Si) from ca. 66.9 % to ca. 83.5 %, and all Z-0.5at-yCTAB samples maintained the proportions of Si(4Si) and Si(3Si, 1Al) regardless of the C_{CTAB} variation, which indicated the nonselective desilication occurred in these samples concerning the decreased Si/Al₂ ratio compared to that of the parent HZSM-11 zeolite. For Z-0.5at-yCTAB the Si/Al₂ ratio increased

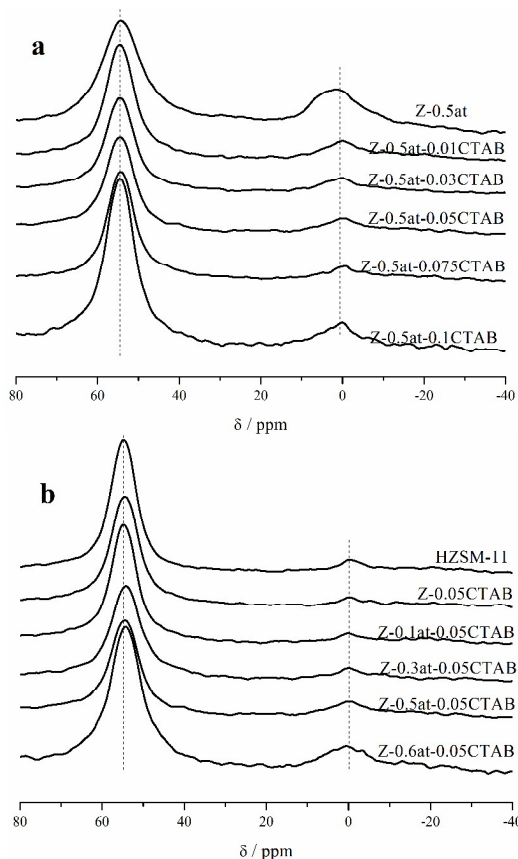


Fig. 3 ^{27}Al MAS NMR spectra of Z-0.5at-yCTAB (a) and Z-xat-0.05CTAB (b) zeolites.

with the increase of C_{CTAB} (Table 1), which was probably ascribed to the effects of washing Al_{ext} out of zeolite or inhibition of realumination by CTAB, since the proportion of Si(4Si) and Si(3Si, 1Al) varied little.

As for Z-xat-0.05CTAB, the proportion of Si(3Si, 1Al) changed little while that of Si(4Si) gradually decreased from 86.4 % (Z-0.05CTAB) to 81.8 % (Z-0.6at-0.05CTAB) with an increase of C_{NaOH} , which illustrated the selective desilication effect of NaOH increased after alkaline treatment³⁵ and was agreement with the Si/Al₂ ratio evolution (Table 1). Besides, the proportion of SiOH for Z-xat-0.05CTAB increased after alkaline treatment and was accordant with S_{BET} , further verified the desilication effect of NaOH.

Morphology characterization

The SEM micrographs for Z-xat-yCTAB were shown in Fig. 5. Z-0.05CTAB zeolite showed a similar morphology to HZSM-11 (Fig. S3). In contrast to the complete disaggregated structure of pure NaOH treated zeolite Z-0.5at (Fig. S3), CTAB addition preserved the spherical aggregated structure obviously. Besides, there was no significant change in morphology of all Z-0.5at-yCTAB series samples. In the cases of Z-xat-0.05CTAB series samples, the size of the spherical aggregated structure showed slight decrease especially in the high C_{NaOH} treated sample (Z-0.6at-0.05CTAB).

TEM images were also shown in Fig. 5. Z-0.05CTAB zeolite exhibited similar micropore arrays with HZSM-11 (Fig. S3),

implying that there was almost no corrosion on the zeolite skeleton. In contrast to the heavily leached surface displayed in Z-0.5at (Fig. S3), well-preserved crystal facets and discrete homogeneously distributed mesopores were shown in Z-0.5at-yCTAB series samples. With the C_{CTAB} increasing from 0.01 to 0.05 M, the mesoporosity features were getting more pronounced. While ZSM-11 zeolite alkaline treated with C_{CTAB} as high as 0.1 M would lead to a slight decrease in the mesoporosity due to the protective effect of CTAB multilayer adsorption, in accordant with the PSD curve as shown in Fig. 1b. Z-0.1at-0.05CTAB showed well preserved crystal, while slightly corrosion of the grain edge could be observed, probably due to smaller nascent mesopores formed most prominently along grain boundaries of the zeolite crystals in the case of mild alkaline treatment⁴⁰. With the increase of C_{NaOH} for Z-xat-0.05CTAB, the mesopore features became prominent, especially for Z-0.6at-0.05CTAB with greater size of mesopores compared with other sample, in agreement with the PSD curve (Fig. 1d).

Compared to the easily amorphized USY and beta zeolites when exposed to alkaline solution²¹, ZSM-11 zeolite was more stable. In our present case, there was no sign for the formation of MCM-41-like OMMs^{22,41} with CTAB addition, in accordance with the TEM and XRD results. Recently, it was reported that CTAB possessed functions to protect the MOR zeolites from uncontrollable and intensive destruction caused by alkaline solution and lead to the formation of mesopores homogeneously distributed along the zeolite crystal⁴², which was accordant with our report.

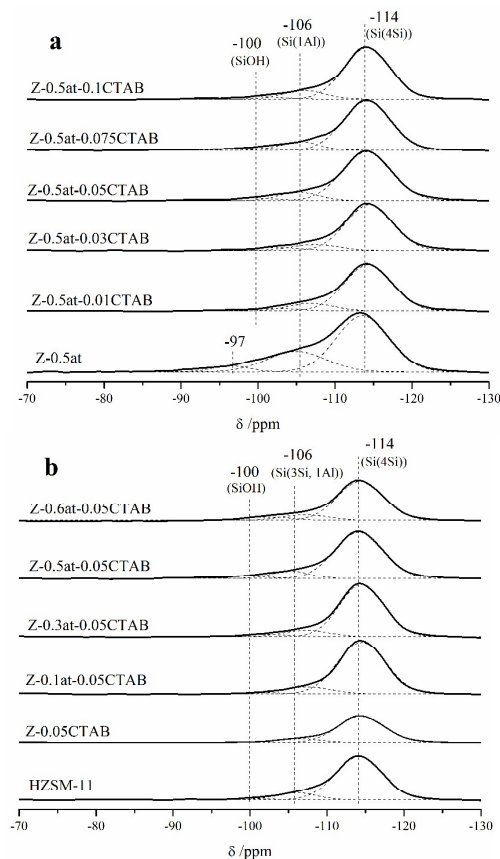


Fig. 4 ^{29}Si MAS NMR spectra of Z-0.5at-yCTAB (a) and Z-xat-0.05CTAB (b) zeolites.

Table 2 Proportion of different Si sites for Z-xat-yCTAB samples.

Samples	Proportion of different Si sites (%)		
	Si(4Si) (-114 ppm)	Si(3Si, 1Al) (-106 ppm)	SiOH (-100, -97 ppm)
HZSM-11	85.9	11.8	2.3
Z-0.05CTAB	86.4	11.0	2.4
Z-0.1at-0.05CTAB	85.9	11.5	2.6
Z-0.3at-0.05CTAB	85.5	10.6	3.8
Z-0.5at-0.05CTAB	83.7	11.6	4.7
Z-0.6at-0.05CTAB	81.8	11.3	6.8
Z-0.5at-0.01CTAB	82.8	12.5	4.7
Z-0.5at-0.03CTAB	83.7	10.9	5.4
Z-0.5at-0.075CTAB	83.6	11.7	4.7
Z-0.5at-0.1CTAB	83.9	12.0	4.1
Z-0.5at	66.9	28.1	5.0

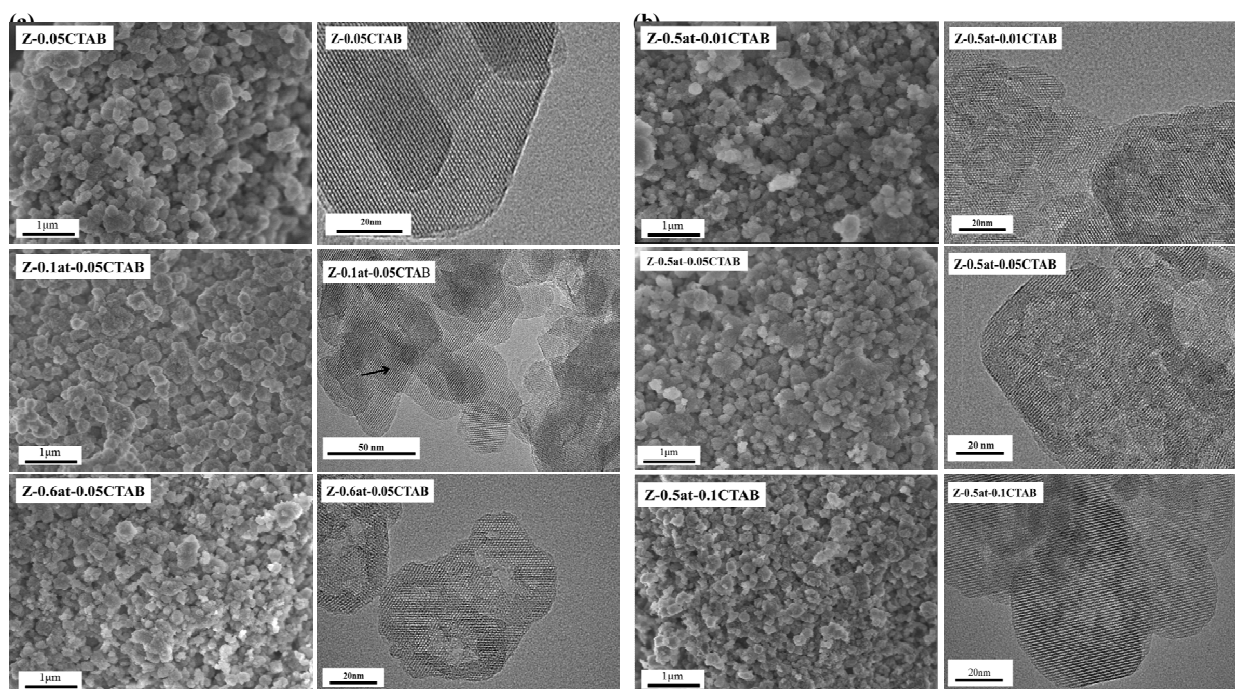
Composite effects of NaOH and CTAB on mesopores production

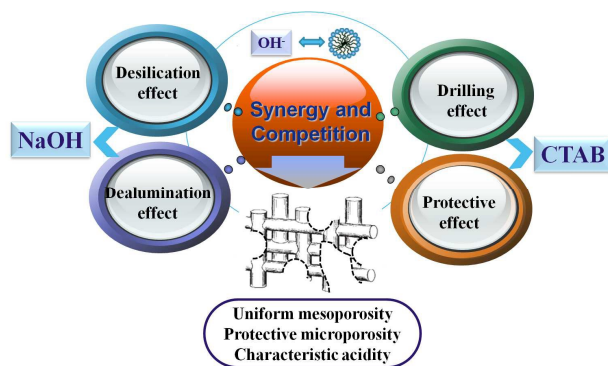
Guided by the above-mentioned characterization results, a possible mesoporosity formation route was proposed as presented in Scheme 1. Since the alkaline treatment in the presence of CTAB is very complicated, the effects of NaOH and CTAB were simplified as follow. On one hand, NaOH treatment leads to a broad PSD via Si extraction (denoted as desilication effect), and simultaneously results in removal of Al species from framework into extra-framework^{35,36}, and these Al_{ext} species could be derived from realumination of Al extracted during alkaline treatment, although there was somehow different from Ref.⁴³ (denoted as dealumination effect). It was demonstrated a clear preferential desilication than dealumination over ZSM-5 during alkaline treatment⁴⁴. On the other hand, in the presence of NaOH, CTAB plays two roles during the alkaline treatment as well. Firstly, CTAB micelles could induce uniform mesopores production with a diameter corresponding to the micelle diameter by drilling effect¹⁸. It should be noticed that the pure CTAB had no drilling effect to produce mesopores, for instance, Z-

0.05CTAB. Secondly, CTAB could adsorb on the external surface of the zeolite to protect the zeolite structure via multilayer adsorption especially when CTAB was in a high concentration⁴⁵, and adsorption of CTAB on the zeolite largely inhibited surface realumination²¹ to be Al_{ext} in this contribution (denoted as protective effect).

In the cases of Z-0.5at-yCTAB (Fig. 1b), with 0.01 M CTAB adding into the solution of 0.5 M NaOH, the intensity of the broad band for BJH curve decreased obviously, accompanying with the formation of a new band centered at ca. 4.2 nm by drilling effect, compared to the pure NaOH treated sample Z-0.5at (Fig. S2). As a matter of convenience, the band centered at ca. 4.2 nm was labeled as Band I, and the broad band with band center greater than 10 nm as Band II. Increasing the C_{CTAB} to 0.03M, the intensity of Band I increased due to the micelle effect enhanced. Further increasing the C_{CTAB}, the intensity of the Band I decreased, especially for Z-0.5at-0.1CTAB, which may be ascribed to that the protective effect of CTAB exceeded the drilling effect at high C_{CTAB}. From Table 1, the intensity of Band II decreased with the increasing C_{CTAB} since the desilication effect of NaOH weakened. Based on these observations, that the desilication effect of NaOH and the drilling and protective effects of CTAB were synergetic and competitive with each other were proposed. It should be noticed that when C_{CTAB} reached to 0.03-0.075 M, these effects may be reach equilibrium, resulting in an approximately stable state of Bands I and II.

As for Z-xat-0.05CTAB (Fig. 1d), the PSD of Z-0.05CTAB was similar to that of HZSM-11, implying that the treatment of ZSM-11 with pure CTAB could not produce mesopores¹⁷. Here, the C_{NaOH} played a significant role during alkaline treatment with CTAB addition. With the increase of C_{NaOH}, the mesoporosity characterization became more and more prominent (Fig. 3). Similarly, the desilication effect of NaOH and the drilling and protective effects of CTAB were synergetic and competitive in these cases. The PSD curve and Si/Al₂ ratio of Z-0.1at-0.05CTAB zeolite showed no obvious change compared with that of HZSM-11, since

**Fig. 5** SEM and TEM images of Z-0.5at-yCTAB (a) and Z-xat-0.05CTAB (b).



Scheme 1 Composite effects of NaOH and CTAB on mesopores production during alkaline treatment with CTAB addition over ZSM-11 zeolite.

the desilication effect was very weak due to the low C_{NaOH} . Under this condition, no abundant mesopores would form, although CTAB was enough to form micelles, as these micelles were likely to adsorb on the surface of zeolite rather than “drilling” into the zeolite. With the C_{NaOH} changing from 0.1 to 0.5 M, the intensity of Bands I and II increased simultaneously, since the desilication effect and drilling effect were synergistic. Further increasing the C_{NaOH} to 0.6 M (Z-0.6at-0.05CTAB), the protective effect of CTAB was not compatible with the desilication effect of NaOH, leading to a sharp increase in the intensity of Band II.

It was noteworthy that Z-0.3at-0.05CTAB showed a weak wide band centered at ca. 3 nm, whose value was slightly less than the 4.2 nm. This may be ascribed to that the desilication effect at C_{NaOH} of 0.3 M was not enough to fully break through the CTAB micelle adsorption layer, leading to the minor appearance in drilling effect. Thereby, the drilling and protective effects of CTAB with certain concentration could be achieved within a certain range of C_{NaOH} . When C_{NaOH} was too low, the drilling effect would not show due to the OH⁻ was not enough to penetrate the CTAB micelle layer like Z-0.1at-0.05CTAB. However, when C_{NaOH} was too high, the protective effect would be broken like Z-0.6at-0.05CTAB, and the zeolite would be corroded seriously.

Maybe, it is helpful to further clarify these effects by ²⁷Al and ²⁹Si MAS NMR spectra. Based on ²⁷Al MAS NMR spectra (Fig. 3), the bands centered at 57 and 0 ppm were integrated and their ratios ($n(\text{Al}_{\text{fra}})/n(\text{Al}_{\text{ext}})$), representing the molar ratios of Al_{fra} to Al_{ext} versus C_{NaOH} and C_{CTAB} were shown in Fig. 6, respectively. For Z-xat-0.05CTAB series sample, the $n(\text{Al}_{\text{fra}})/n(\text{Al}_{\text{ext}})$ decreased linearly with the increase of C_{NaOH} . While in the cases of Z-0.5at-yCTAB series sample, the $n(\text{Al}_{\text{fra}})/n(\text{Al}_{\text{ext}})$ increased slowly with the increasing C_{CTAB} . Combined the ²⁷Al spectra with ²⁹Si spectra (Figs. 3 and 4, Table 2), during the alkaline treatment NaOH had a desilication effect accompanying the realumination effect, to be Al_{ext} of this contribution. While CTAB showed a protective effect on zeolite structure (Al_{fra} , Si(3Si,1Al)) accompanied by the function of washing Al_{ext} or inhibiting realumination²¹. Therefore, for Z-0.5at-yCTAB the protective effect of CTAB was strengthened with the increase of C_{CTAB} and the desilication effect of NaOH was weakened, leading to the increased $n(\text{Al}_{\text{fra}})/n(\text{Al}_{\text{ext}})$, in contrast to the cases of Z-xat-0.05CTAB with the increase of C_{NaOH} .

Acidity characterization

The Py-IR technique was employed to compare the total acidity of Z-xat-yCTAB samples. The spectra of Z-xat-yCTAB were shown in Fig. S4 and the corresponding acid concentrations were summarized in Table 3. For convenience, the ratio of Brønsted to Lewis acid

concentration of total acidity detected at 150 °C, that with strong strength detected at 450 °C, and that with weak-medium strength were denoted as $B/L_{\text{Py-150}}$, $B/L_{\text{Py-450}}$ and $B/L_{\text{Py-WM}}$, respectively. As shown in Table 3, the $B/L_{\text{Py-150}}$ value on all Z-xat-yCTAB zeolites maintained at ca. 1.00, indicating that the alkaline treatment in the presence of CTAB would not change the B/L of the total acidity.

On the other hand, the $B/L_{\text{Py-450}}$ of Z-xat-0.05CTAB series samples decreased from 4.57 to 1.41 with the increase of C_{NaOH} , while the $B/L_{\text{Py-450}}$ of Z-0.5at-yCTAB series samples slowly increased from 1.39 to 2.19 with C_{CTAB} increasing from 0.01 to 0.1 M. According to the results in Table 3, for all Z-xat-yCTAB series samples, the ratio of $B/L_{\text{Py-450}}$ increased with the increase of the proportion of C_{CTAB} in the NaOH and CTAB mixture ($C_{\text{CTAB}}/(C_{\text{CTAB}}+C_{\text{NaOH}})$). Besides, it was interesting to find that $B/L_{\text{Py-450}}$ showed correlation with $n(\text{Al}_{\text{fra}})/n(\text{Al}_{\text{ext}})$ to some extent (Fig. S5). The high value of B/L with strong strength in zeolite might be ascribed to the high concentration of Al_{fra} with tetrahedral coordination⁴⁶. As described before, CTAB could protect the Al_{fra} and wash some Al_{ext} species (Lewis acid sites⁸) out of the zeolite crystal (Fig. 3), and inhibited the realumination during alkaline treatment²¹. While NaOH treatment had the opposite effects, i.e. decreasing Brønsted acid concentration and increasing Lewis acid concentration^{47, 48}. Thereby, it was not difficult to understand that $B/L_{\text{Py-450}}$ increased accordingly with $C_{\text{CTAB}}/(C_{\text{CTAB}}+C_{\text{NaOH}})$. This also supported the synergistic and competitive relationships between the effects of NaOH and CTAB, as proposed above.

As for $B/L_{\text{Py-WM}}$, the value for Z-0.5at-yCTAB increased from 0.56 to 0.75 with the C_{CTAB} ranging from 0.01 to 0.05M, and then decreased with higher C_{CTAB} treatment. Similarly, in the cases of Z-xat-0.05CTAB, $B/L_{\text{Py-WM}}$ value first increased and then decreased with the increasing C_{NaOH} . Therein, Z-0.05CTAB showed a $B/L_{\text{Py-WM}}$ value of 0.16, similar to that of HZSM-11. Since the NaOH treatment would produce some protonic sites with weaker acid strength than typical zeolitic Si-OH-Al groups¹², which were likely situated on the mesopore surface³⁰. With the increase of C_{NaOH} from 0.1 to 0.5 M, the $B/L_{\text{Py-WM}}$ value of Z-xat-0.05CTAB increased with mesopores production. However, higher C_{NaOH} (0.6 M) treatment would bring about a higher mesoporosity accompanying with the slight destruction of zeolite structure, leading to a lower $B/L_{\text{Py-WM}}$ value. In the cases of Z-0.5at-yCTAB, with the increase of C_{CTAB}

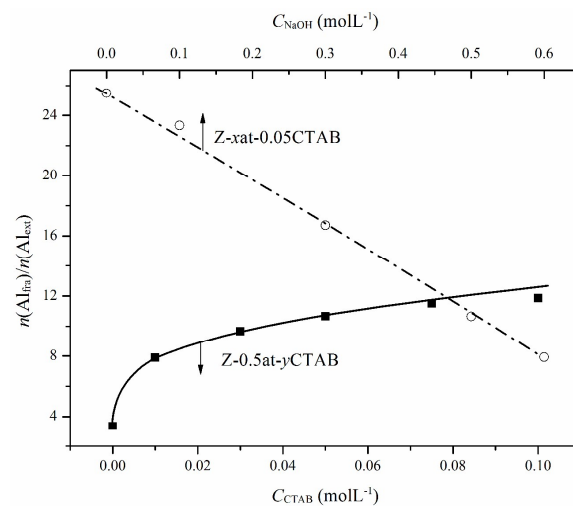


Fig. 6 Relationship between the ratios of $n(\text{Al}_{\text{fra}})/n(\text{Al}_{\text{ext}})$ and concentrations of alkaline and CTAB for Z-xat-0.05CTAB and Z-0.5at-yCTAB.

Table 3 Acidity Characterization results measured by FT-IR techniques of Z-xat-yCTAB.

Samples	Concentration ($\mu\text{mol g}^{-1}$) and ratio of acid sites									Determined with pivalonitrile ^d		
	Determined with pyridine						Strong _{py-450} ^c					
	Total _{py-150} ^a			WM _{py-150-450} ^b			Strong _{py-450} ^c			C_{B-Pn}	C_{L-Pn}	B/L_{Pn}
	$C_{B-Py-150}$ ^d	$C_{L-Py-150}$ ^e	B/L _{-Py-150}	$C_{B-Py-WM}$	$C_{L-Py-WM}$	B/L _{-Py-WM}	$C_{B-Py-450}$	$C_{L-Py-450}$	B/L _{-Py-450}			
Z-0.5at	190	202	0.94	95	106	0.90	95	96	0.99	98	23	4.3
Z-0.5at-0.01CTAB	181	183	0.99	50	89	0.56	131	94	1.39	120	31	3.9
Z-0.5at-0.03CTAB	179	190	0.94	65	109	0.60	114	81	1.41	113	33	3.4
Z-0.5at-0.05CTAB	165	155	1.06	65	87	0.75	100	68	1.47	114	32	3.6
Z-0.5at-0.075CTAB	162	192	0.84	52	118	0.44	110	74	1.49	- ^g	-	-
Z-0.5at-0.1CTAB	143	142	1.01	27	89	0.30	116	53	2.19	101	27	3.7
HZSM-11	151	106	1.42	12	76	0.16	139	30	4.63	1	5	0.2
Z-0.05CTAB	120	116	1.03	15	93	0.16	105	23	4.57	9	5	1.8
Z-0.1at-0.05CTAB	131	132	0.99	21	94	0.22	110	38	2.90	53	15	3.5
Z-0.3at-0.05CTAB	149	139	1.07	20	78	0.26	129	61	2.11	112	29	3.9
Z-0.6at-0.05CTAB	146	154	0.95	47	84	0.56	99	70	1.41	123	34	3.6

^aTotal_{py-150}: Total acid concentration determined by Py-IR technique at 150 °C.

^bWM_{py-150-450}: Weak-medium acid concentration was defined as the difference between the Total_{py-150} and Strong_{py-450}.

^cStrong_{py-450}: Strong acid concentration determined by Py-IR technique at 450 °C.

^d C_B : Brønsted acid concentration.

^e C_L : Lewis acid concentration.

^fThe extinction coefficient of the IR bands of pivalonitrile interacting with both Brønsted ($0.11 \text{ cm}^2 \mu\text{mol}^{-1}$) and Lewis ($0.16 \text{ cm}^2 \mu\text{mol}^{-1}$) acid sites was reported in reference ¹³.

^g -: Not determined.

from 0.01 to 0.05 M, the drilling effect of CTAB micelles would increase and induce forming more mesopores centered at 4.2 nm, leading to the increase in B/L_{Py-WM} value. However, higher C_{CTAB} would well protect the zeolite structure, leading to a slight reduction in mesoporosity (Fig. 5 and Table 1), then a decrease in the ratio of

B/L_{Py-WM} . It should be noticed that the intensity of mesopores centered ca. 4.2 nm first increased and then decreased (Fig. 1b), leading to the corresponding change of B/L_{Py-WM} value, even though the V_{meso} of Z-0.5at-yCTAB did not change a lot with the increasing C_{CTAB} (Table 1). These were somehow different from the cases of Z-xat³⁰, which was probably ascribed to the effects of NaOH and CTAB on physiochemical properties of resultant samples.

It should be noticed that in this work the acidity was focused on the B/L ratios with different acid strengths rather than the acid concentrations, and was somehow different from the Ref. ⁴⁹, which reported that depending on the severity of the initial alkaline treatment, the samples exhibited an appreciably reduced number of Brønsted acid sites (20 % - 30 %) and a significantly increased concentration of Lewis acid sites (4 - 4.5 fold). This may be ascribed to that the composite effects of NaOH and CTAB were different from the single effect of NaOH.

The acidity of external surface for hierarchical zeolite is an important property. Therefore, the acidity of external surfaces and the accessibility factor (AF)¹³ of Z-xat-yCTAB were investigated by Pn-IR technique, and the definition of AF was shown in experimental section. The normalized and deconvoluted of Pn-IR spectrum for Z-0.5at-0.05CTAB zeolite was shown in Fig. S6a, and the Pn-IR spectra of Z-xat-yCTAB series samples were presented in Fig. S6b. The concentrations of Brønsted (C_{B-Pn}) and Lewis (C_{L-Pn}) acid sites were calculated according to Ref. ¹³ and listed in Table 3. The acid sites accessible to Pn on Z-0.5at-yCTAB changed little with the increasing C_{CTAB} . With respect to Z-xat-0.05CTAB ($x > 0$), the C_{B-Pn} increased from 9 to 123 $\mu\text{mol g}^{-1}$ and C_{L-Pn} increased from 5 to 34 $\mu\text{mol g}^{-1}$ with the increase of C_{NaOH} . Both cases obtained a similar B/L_{Pn} value. For all Z-xat-yCTAB series samples, B/L_{Pn} value was higher than B/L_{Py-150} (including Z-0.05CTAB).

The evolution of AF with the C_{NaOH} and C_{CTAB} was shown in Fig. 7, respectively. The AF_B was higher than the AF_L on the whole. For Z-0.5at-yCTAB (Fig. 7a), AF_B and AF_L values kept constant at ca. 69 % and ca. 19 %, respectively, regardless of the variation of C_{CTAB} . While for Z-xat-0.05CTAB (Fig. 7b), Z-0.05CTAB exhibited very low AF_B (7.5 %) and AF_L (4.3 %), which was in accordance with its low V_{meso} . With the increase of C_{NaOH} , the AF_B and AF_L

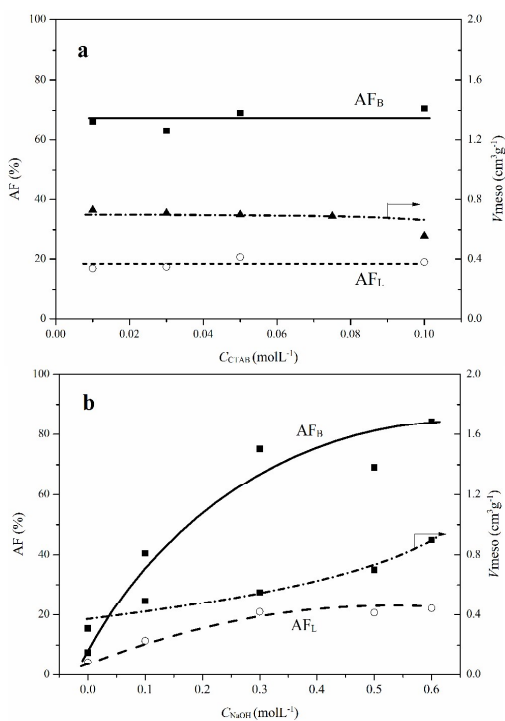


Fig. 7 Accessibility factor (AF) and mesopore volume as a function of alkaline concentration on Z-0.5at-yCTAB (a) and Z-xat-0.05CTAB (b) samples.

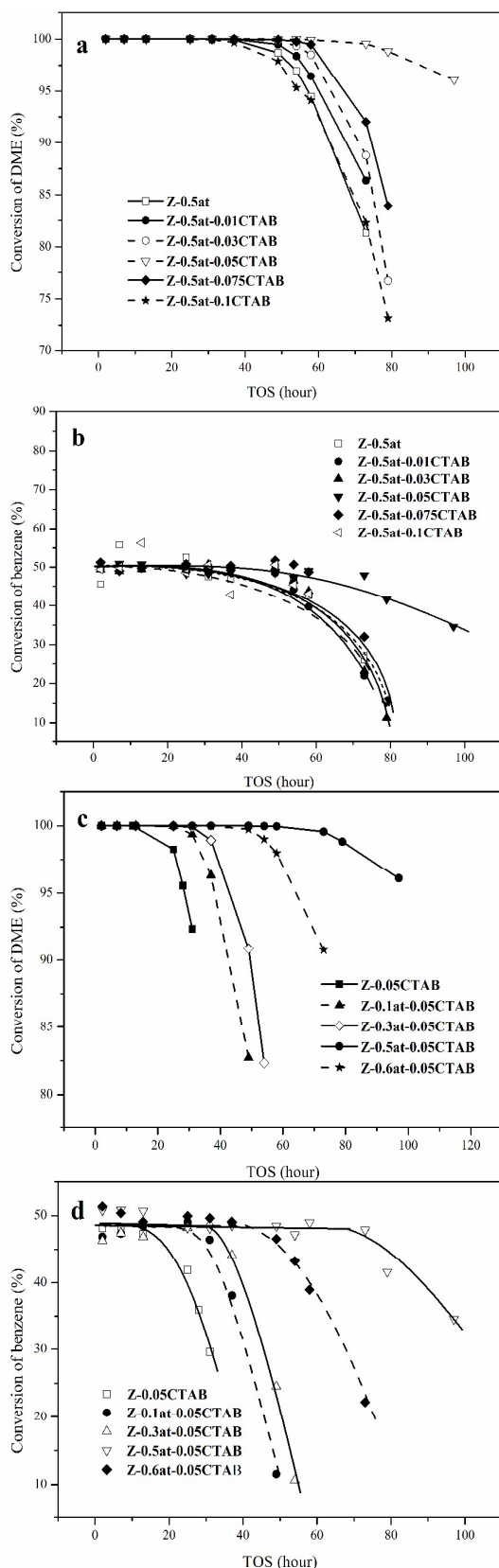


Fig. 8 Reaction stability on Z-0.5at-yCTAB (a, b) and Z-xat-0.05CTAB (c, d) zeolite catalysts.

increased to ca. 78 % and ca. 21 %, respectively. As expected, AF of both Z-0.5at-yCTAB and Z-xat-0.05CTAB showed good correlation with the mesoporosity (Fig. 7), in accordance with the cases of ZSM-5 treated with NaOH and TBAOH¹³. While for Z-xat-0.05CTAB the evolution of AF with C_{NaOH} was different from that of Z-0.5at³⁰, which should be related with specific role of CTAB.

Reaction performance

The reaction performances of selected samples were evaluated in the alkylation of benzene with DME. This alkylation is catalyzed by the Brønsted acid sites of ZSM-5²⁹ and ZSM-11^{28,30,50}, on which the methoxy species, as an important agent for benzene methylation, are formed from the dissociation of DME. Since the similar zeolite topology results in similar product distribution⁵¹, almost the same initial product distributions could be obtained over NaOH treated (Z-0.5at) and mixed solution of NaOH and CTAB treated (Z-xat-yCTAB) zeolite catalysts.

The selectivity of the main products over Z-0.5at-0.05CTAB was shown in Fig. S7. During 93 h of TOS, the selectivities of dry gas (< 1 %) and LPG (< 2 %) over Z-0.5at-0.05CTAB were very low, and the selectivity of the liquid products was as high as ca. 98 %. Toluene and xylene were the main liquid products, similar to the case of ZSM-5²⁹. The toluene selectivity exhibited an increased trend with TOS. The selectivities of xylene, trimethylbenzene, C₅₋₆ and propylbenzene almost kept constant within 2-73 h of TOS and then decreased (TOS = 73-93 h), while those of ethylbenzene and ethyltoluene decreased with TOS. The possible reaction route was illustrated previously³⁰.

The stability of different ZSM-11 catalysts was shown in Figs. 8a and 8c, in terms of DME conversion; as well as in Figs. 8b and 8d, in terms of benzene conversion. The scattering of benzene conversion data is very likely due to the fluctuation in the evaporation of benzene²⁹. The initial conversions (the conversions at 2 h of TOS) of benzene and DME over all sample tested were ca. 48 % and 100 %, respectively. As shown in Figs. 8a and 8b, increasing the C_{CTAB} from 0.01 to 0.1 M over Z-0.5at-yCTAB, the stability based on the conversions of DME and benzene first increased and then decreased. Meanwhile, the reaction stability of Z-xat-0.05CTAB series samples was also investigated as shown in Figs. 8c and 8d. It increased with C_{NaOH} changing from 0 to 0.5 M, and decreased when C_{NaOH} was further raised to 0.6 M. Among all samples tested, Z-0.5at-0.05CTAB exhibited the best performance. The stability of the as prepared ZSM-11 catalysts followed the sequence as Z-0.5at-0.05CTAB > Z-0.5at > HZSM-11, similar to that over ZSM-5 zeolite treated with NaOH and CTAB in MTH reaction^{8,9}.

Relations of reaction performance with physicochemical properties

As shown in Fig. 8, the initial DME and benzene conversions were quite similar, while the reaction stability was demonstrated remarkably different on all tested ZSM-11 catalysts. Here, the relations of reaction performance with acidity and mesostructural properties of the catalysts were investigated. For the sake of convenient comparison, the T_{D} (TOS when DME conversion was at 95 %) and T_{B} (TOS when benzene conversion was at 34 %) were taken as indexes of the reaction stability.

As shown in Fig. 9a, increasing the C_{CTAB} from 0.01 to 0.1 M, the stability of Z-0.5at-yCTAB first increased and then decreased, and Z-0.5at-0.05CTAB showed the best one with its stability of 100 h for T_{D} and 100 h for T_{B} , which could be deduced by the extended line in Figs. 8a and 8b. Similar phenomenon also appeared in the cases of Z-xat-0.05CTAB with C_{NaOH} variation from 0 to 0.6 M (Fig. 9b). In this paper, it was interesting to find that the stability on the resulting hierarchical zeolite catalysts was relevant well to the

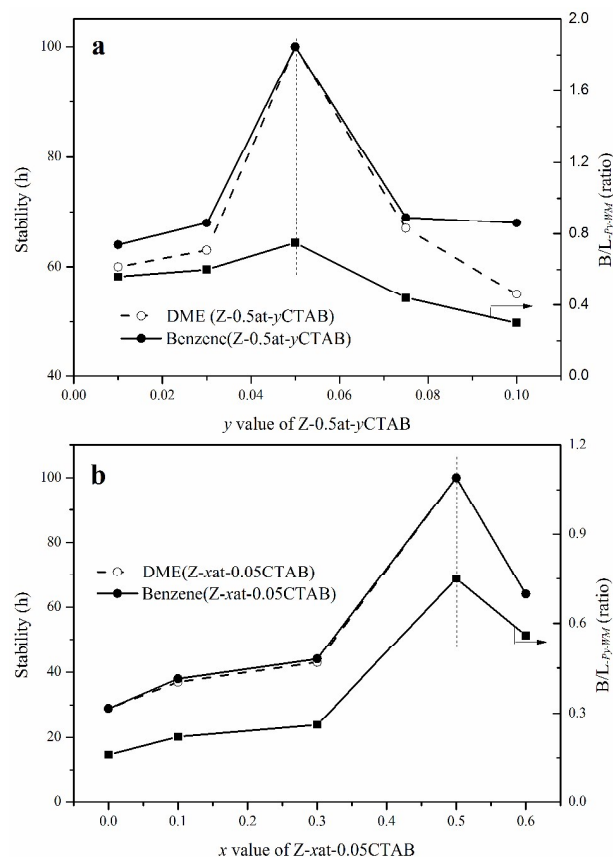


Fig. 9 Variation of stability and weak-medium acidity detected by Py-IR of Z-0.5at-yCTAB (a) and Z-xat-0.05CTAB (b) catalysts.

B/L_{Py-IR} ratio (Fig. 9). It should be noted that there did not exist well relationship between the stability and the mesoporosity, hierarchy factor and AF as previous Refs.^{26, 52}. This was different from the cases of ZSM-11 samples treated with pure NaOH (Z-xat), where both the concentrations with weak-medium strength and mesoporosity of Z-xat showed good consistence with the reaction stability³⁰.

As shown in Table 1, the microporosity and mesoporosity of Z-0.5at-yCTAB zeolites had no obvious change. While for Z-xat-0.05CTAB series samples, with the increase of C_{NaOH} , there existed a slight decrease in the microporosity meanwhile a linear increase in the mesoporosity. This could be ascribed to the protective effect and drilling effect of CTAB^{18, 33}, leading to an effective mesoporosity generation and a minor expense of microporosity.

As reported, the higher mesoporosity is beneficial to the superior stability⁴. In the cases of Z-0.5at-yCTAB, due to the similar mesoporosity among these samples, a similar effect on the diffusion

of coke precursors from the micro/mesopores to the external surfaces could be obtained. The reaction stability of Z-xat-0.05CTAB was generally in accord with V_{meso} , except for Z-0.6at-0.05CTAB, whose V_{meso} was higher, while an inferior reaction stability was achieved compare to Z-0.5at-0.05CTAB. As we know, the effects of zeolite catalysts on reaction performance are very complicated, and the major factors are acidity and structural properties in general^{4, 9, 30}. In our present work, owing to the composite effects of NaOH and CTAB, the structural property on reaction stability was weakened, and then the acidity became the crucial factor. Combined with the acidity as shown in Fig. 9, Z-0.5at-0.05CTAB sample possessing the best reaction performance was reasonable.

DME-to-olefin reaction is favored by the weak acidity as the Brønsted acid sites have the ability to bind the methoxy species, and the weak acid intensities are beneficial to reduce hydrogen transfer reaction rate, lowering formation rate of coke and heavy hydrocarbons^{53, 54}. Moreover, the higher Si/Al₂ ratio was obtained by CTAB addition, which may affect the availability of active sites, and then the ratio of B/L played a role on reaction performance in the alkylation of benzene reaction⁵⁵.

To sum up, in our paper the composite effects of NaOH and CTAB modification weakened the role of mesoporosity on reaction stability, besides mildly regulated the acidity of Z-xat-yCTAB zeolites. Under this circumstance, it was the ratio of B/L_{Py-IR} that became the decisive factor on reaction performance in alkylation of benzene with DME.

Differences between alkaline treatment with CTAB and TPABr

Alkylammonium cations were highly suitable pore-directing agents²¹. In this work, two representative agents of CTAB and TPABr were selected, and samples treated with NaOH and TPABr were prepared under the same conditions as those treated with NaOH and CTAB. The physicochemical data of resultant samples were listed in Table 4. Z-0.05TPABr showed similar RC, Si/Al₂ ratio, solid yield and N₂ isotherm to Z-0.05CTAB. While with the increase of C_{NaOH} , Z-xat-0.05TPABr exhibited reduced yield, Si/Al₂ ratio and RC, as the adsorbed TPABr layer could not resist the increased corrosion from high concentration of NaOH. These were in accord with the cases of Z-xat-0.05CTAB samples, but CTAB demonstrated stronger ability to protect zeolite structure than TPABr under relatively high C_{NaOH} . The N₂ isotherms of Z-xat-0.05TPABr ($x = 0.2, 0.28$ and 0.35) samples (Fig. 10a) showed significantly increased uptake at $P/P_0 = 0.4-1.0$, except for the large uptake at low P/P_0 . These consequently gave rise to PSDs centered at 4 - 7 nm range (Fig. 10b). When C_{NaOH} was increased to 0.5 M, the N₂ isotherm of the sample (Z-0.5at-0.05TPABr) displayed a more obvious uptake at $P/P_0 > 0.6$. This indicated the generation of greater mesopores, which was verified by the presence of a clear band centered at ca. 30 nm (Fig. 10b). The effect of C_{TPABr} was also investigated under 0.5 M of C_{NaOH} . Compared to Z-0.5at-0.05TPABr, Z-0.5at-0.1TPABr showed slightly higher solid yield, Si/Al₂ ratio and RC. Besides, the N₂ isotherm of Z-0.5at-0.1TPABr showed a sharp increased uptake at $P/P_0 > 0.5$,

Table 4 Textural and physicochemical data of ZSM-11 samples treated with NaOH and CTAB/TPABr.

Samples	Yield (%)	Si/Al ₂	RC (%)	Textural data			
				S_{BET} (m ² g ⁻¹)	S_{ext} (m ² g ⁻¹)	V_{micro} (cm ³ g ⁻¹)	V_{meso} (cm ³ g ⁻¹)
Z-0.05CTAB	89	57	106	381	115	0.121	0.314
Z-0.5at-0.05CTAB	58	40	89	523	281	0.109	0.706
Z-0.05TPABr	91	57	108	372	116	0.121	0.308
Z-0.2at-0.05TPABr	67	47	96	523	276	0.111	0.569
Z-0.28at-0.05TPABr	59	41	87	560	311	0.111	0.715
Z-0.35at-0.05TPABr	48	35	76	565	328	0.105	0.816
Z-0.5at-0.05TPABr	30	22	61	517	325	0.092	1.323
Z-0.5at-0.1TPABr	34	26	70	550	329	0.093	1.219

Table 5 Acidity Characterization results determined by Py-IR and reaction activity of ZSM-11 samples treated with NaOH and CTAB/TPABr.

Samples	Concentration ($\mu\text{mol g}^{-1}$) and ratio of acid sites									Reaction activity	
	$C_{B-Py-150}$	$C_{L-Py-150}$	B/L	$C_{B-Py-WM}$	$C_{L-Py-WM}$	B/L	$C_{B-Py-450}$	$C_{L-Py-450}$	B/L	$X_{DME} (\%)^a$	$X_{Benzene} (\%)^a$
			$-Py-150$			$-Py-WM$			$-Py-450$		
Z-0.05CTAB	120	116	1.03	15	93	0.16	105	23	4.57	-	-
Z-0.5at-0.05CTAB	165	155	1.06	65	87	0.75	100	68	1.47	96.13	35.30
Z-0.05TPABr	128	142	0.90	19	92	0.21	109	50	2.18	-	-
Z-0.2at-0.05TPABr	158	125	1.26	10	38	0.26	148	87	1.70	84.03	20.91
Z-0.28at-0.05TPABr	186	136	1.37	19	46	0.41	167	90	1.86	97.37	38.88
Z-0.35at-0.05TPABr	175	115	1.52	27	40	0.67	148	75	1.97	94.97	34.49
Z-0.5at-0.05TPABr	163	121	1.35	117	67	1.75	66	54	1.22	89.12	24.41
Z-0.5at-0.1TPABr	187	94	1.99	107	56	1.91	80	38	2.11	94.47	32.48

^a X_{DME} and $X_{Benzene}$: Conversion of DME and that of benzene at TOS of 6 h under the conditions of 350 °C, 0.1 MPa, $n(\text{benzene})/n(\text{DME}) = 2$, and the DME WHSV of 32 h^{-1} .

which corresponded to the significant band centered at ca. 20 nm in the BJH curve (Fig. 10b).

On the other hand, Z-0.05TPABr had similar textural data to Z-0.05CTAB. As for Z-xat-0.05TPABr, the V_{micro} gradually decreased from 0.111 to 0.092 $\text{cm}^3 \text{g}^{-1}$ and V_{meso} remarkably increased from 0.569 to 1.323 $\text{cm}^3 \text{g}^{-1}$, with C_{NaOH} varying from 0.2 to 0.5 M. Additionally, during alkaline treatment, higher TPABr concentration (denoted as C_{TPABr}) addition led to smaller mesopore size, lower V_{meso} and higher V_{micro} (Z-0.5at-0.1TPABr vs Z-0.5at-0.05TPABr), which

could be ascribed to the protection effect of TPABr upon zeolite structure.

Compared to Z-0.5at-0.05CTAB, Z-0.5at-0.05TPABr showed obviously lower solid yield (30 % vs 58 %), Si/Al₂ ratio, RC and V_{micro} , higher V_{meso} and greater mesopore size. With the decrease of C_{NaOH} from 0.5 to 0.2 M, Z-xat-0.05TPABr displayed increased solid yield from 30 % to 67 %, while for Z-xat-0.05CTAB, the solid yield varied from 41 % to 74 % with the decrease of C_{NaOH} from 0.6 to 0.1 M. This changing trend also happened in the cases of Si/Al₂ ratio, RC and V_{micro} , respectively, for the two series samples. In fact, Z-0.28at-0.05TPABr exhibited similar solid yield (59 % vs 58 %), Si/Al₂ ratio and RC to Z-0.5at-0.05CTAB. Namely, to make the sample alkaline treated with TPABr and that with CTAB have similar solid yields, it was necessary to choose lower C_{NaOH} for the former. This may be attributed to the fact that the monolayer adsorption of TPABr protected zeolite structure less effectively than the multilayer adsorption of CTAB, and TPABr with shorter alkyl chains may form a less closely packed adsorption layer than CTAB²¹.

The acidity of TPABr series samples was assessed by Py-IR technique and the acid concentrations and their ratios with different strengths of selected samples were summarized in Table 5. Z-0.05TPABr displayed a similar acidity to Z-0.05CTAB. As to Z-xat-0.05TPABr samples, both the total ($C_{B-Py-150}$) and strong ($C_{B-Py-450}$) Brønsted acid concentrations first increased and then decreased with the increase of C_{NaOH} , and the highest value appeared on Z-0.28at-0.05TPABr. This changing trend was in consistent with that of Z-xat samples³⁰. As for B/L of Z-xat-0.05TPABr, both B/L_{-Py-150} and B/L_{-Py-450} first increased a little and then decreased, while B/L_{-Py-WM} gradually increased, with C_{NaOH} varying from 0.2 to 0.5 M. Compared to Z-0.5at-0.05TPABr, Z-0.5at-0.1TPABr showed higher B/L at any strength, which was different from the situation of CTAB series samples (Table 3). This further demonstrated that different surfactants had various influences on the properties of alkaline treated samples, which could be attributed to their different adsorption properties and protective effects upon zeolite.

Also, the alkylation reaction of benzene with DME was investigated over the samples alkaline treated with TPABr, and the DME and benzene conversions at TOS of 6 h were defined as reaction activity (Table 5). For Z-xat-0.05TPABr samples, with the increase of C_{NaOH} , the reaction activity first increased and then decreased, and Z-0.28at-0.05TPABr displayed the highest activity with DME conversion of 97.37 % and benzene conversion of 38.88 %. Also, Z-0.5at-0.1TPABr showed higher activity than Z-0.5at-0.05TPABr. This was related to their acidity and structural properties^{22, 56}. Z-0.5at-0.05TPABr displayed lower activity than Z-0.5at-0.05CTAB, which might be related to more serious collapse of structure for the former than the latter. While for Z-0.28at-0.05TPABr and Z-0.5at-0.05CTAB, with similar solid yields, Si/Al₂

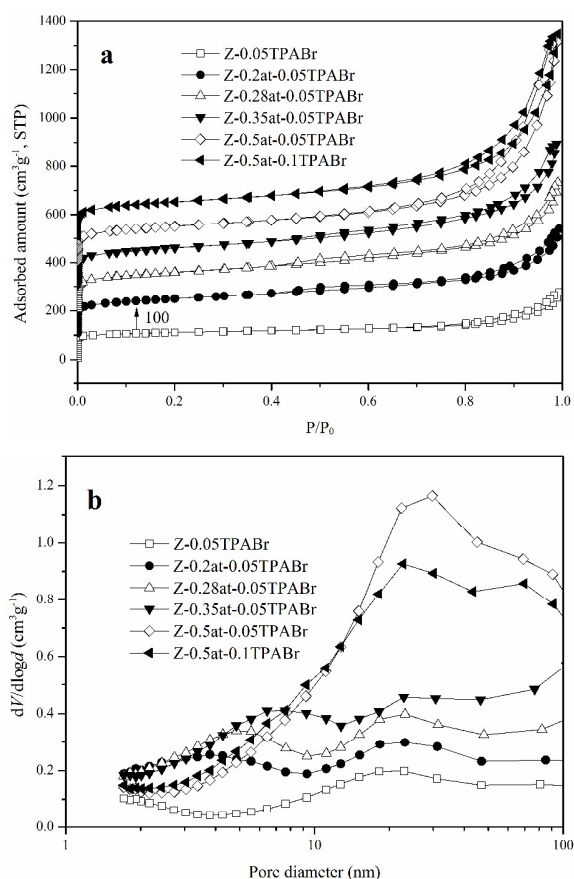


Fig. 10 Nitrogen adsorption and desorption isotherms at -196 °C (a); and BJH pore size distribution plots derived from the adsorption branch (b) for Z-0.05TPABr, Z-0.2at-0.05TPABr, Z-0.28at-0.05TPABr, Z-0.35at-0.05TPABr, Z-0.5at-0.05TPABr and Z-0.5at-0.1TPABr.

ratios and RC, they exhibited comparable reaction activity. This indicated that either CTAB or TPABr could be used as an additive during alkaline treating ZSM-11, but different C_{NaOH} was preferred for both additives. By the way, all tested samples had a similar product distribution (not shown).

J. Pérez-Ramírez et al.²² reported that USY and beta treated with NaOH and TPABr (non-micelle forming) did not lead to composites but highly crystalline hierarchical zeolites, while those prepared with NaOH and CTAB (micelle forming) displayed the composites (zeolite/OMMs) generation. The former exhibited superior performance than the latter in the alkylation of toluene with 2-propanol or benzyl alcohol. That was somehow different from our work. It may be ascribed to the different intrinsic qualities of CTAB and TPABr²¹ and different alkaline treatment conditions, which had evident effects on the acidity and structural properties of resultant samples, just as MCM-49 based micro-mesoporous composites and hierarchical MCM-49 zeolite with intracrystalline mesopores could be obtained by treating MCM-49 in solution with NaOH and CTAB under different treatment conditions, respectively^{33, 57}. Under our treatment conditions, the ZSM-11 samples alkaline treated with assistance of CTAB were hierarchical ZSM-11 with intracrystalline mesopores, well protected micropores meanwhile without OMMs production, in spite of the micelle forming nature of CTAB.

Conclusion and Outlook

The facile alkaline treatment of ZSM-11 zeolites by mixed NaOH and CTAB (Z-xat-yCTAB) was performed. Physiochemical properties showed that Z-xat-yCTAB zeolites had higher Si/Al₂ ratio and RC, uniform mesoporosity and well protective microporosity compared with the pure NaOH treated zeolites.

The composite effects of NaOH and CTAB on mesoporosity formation were proposed. NaOH mainly induces desilication and produces extra-framework Al, while the CTAB has two roles of drilling effect and protective effect in the alkaline solution. Combined with the TEM images, BJH curves as well as ²⁹Si and ²⁷Al MAS NMR results, the synergetic and competitive effects between the CTAB and NaOH during alkaline treatment were proposed. As for CTAB with a certain concentration, if C_{NaOH} was too low, the drilling effect would not show, however, if C_{NaOH} was too high, the protective effect of CTAB would be broken.

The acidity of Z-xat-yCTAB series samples was investigated systematically. Pyridine-IR measurement revealed the B/L ratios of total acidity for all the samples obtained were quite similar to each other, while those with strong strength slowly increased with the $C_{\text{CTAB}}/(C_{\text{CTAB}}+C_{\text{NaOH}})$. As to the B/L ratios with weak-medium strength for Z-0.5at-yCTAB and Z-xat-0.05CTAB, they firstly increased and then decreased with the increasing C_{CTAB} or C_{NaOH} . Besides, Pivalonitile-IR measurement exhibited that all Z-xat-yCTAB ($x > 0$) zeolites had the similar B/L ratios of external surface acidity. In addition, the evolutions of AF with an increase of C_{NaOH} and C_{CTAB} of Z-xat-yCTAB were in line with those of mesoporosity.

When Z-xat-yCTAB series samples were used as catalysts in the alkylation of benzene with DME, they presented significantly better reaction stability compared to ZSM-11 treated with pure NaOH, in spite of the roughly similar product distributions. For Z-xat-yCTAB catalysts the B/L ratio with weak-medium strength displayed well correlation with the reaction stability, meanwhile the mesoporosity did not make a great difference. Perhaps, the interplay of NaOH and CTAB modification weakened the effect of structural property and regulated the acidity properly of Z-xat-yCTAB samples.

TPABr could also be used as an additive during alkaline treating ZSM-11, but NaOH concentration was different from the case of using CTAB as the additive to obtain resultant samples with comparable solid yield, Si/Al₂ ratio, RC and alkylation performance.

This was mainly attributed to the different adsorption properties and protective effects upon zeolites of both alkylammonium cations.

Our results provided valuable insights regarding the hierarchical zeolites obtained from alkaline treatment in the presence of CTAB as well as TPABr, aided our understanding of their physiochemical implication, and highlighted their potential in catalyzed reactions. Furthermore, it is very important to develop a sustainable approach to prepare hierarchical zeolites. In the further work, we will take advantage of the costly zeolite removed by alkaline treatment, recycle the waste streams and prevent the organic compounds from combustion as J. Pérez-Ramírez et al.⁵⁸ stated.

Acknowledgements

The guidance and help of Professor Yide Xu is greatly appreciated.

References

- 1 Y. Tao, H. Kanoh and K. Kaneko, *Adsorption*, 2006, **12**, 309-316.
- 2 H. Zhu, Z. Liu, D. Kong, Y. Wang and Z. Xie, *J. Phys. Chem. C*, 2008, **112**, 17257-17264.
- 3 J. Li, X. Li, G. Zhou, W. Wang, C. Wang, S. Komarneni and Y. Wang, *Appl. Catal. A*, 2014, **470**, 115-122.
- 4 J. Kim, M. Choi and R. Ryoo, *J. Catal.*, 2010, **269**, 219-228.
- 5 J. Pérez-Ramírez, S. Abelló, A. Bonilla and J.C. Groen, *Adv. Funct. Mater.*, 2009, **19**, 164-172.
- 6 D.P. Serrano, J.M. Escola and P. Pizarro, *Chem. Soc. Rev.*, 2013, **42**, 4004-4035.
- 7 K. Mlekodaj, K. Tarach, J. Datka, K. Góra-Marek and W. Makowski, *Microporous Mesoporous Mater.*, 2014, **183**, 54-61.
- 8 F. Schmidt, C. Hoffmann, F. Giordanino, S. Bordiga, P. Simon, W. Carrillo-Cabrera and S. Kaskel, *J. Catal.*, 2013, **307**, 238-245.
- 9 F. Schmidt, M.R. Lohe, B. Büchner, F. Giordanino, F. Bonino and S. Kaskel, *Microporous Mesoporous Mater.*, 2013, **165**, 148-157.
- 10 W.C. Yoo, X. Zhang, M. Tsapatsis and A. Stein, *Microporous Mesoporous Mater.*, 2012, **149**, 147-157.
- 11 K. Tarach, K. Góra-Marek, J. Tekla, K. Brylewska, J. Datka, K. Mlekodaj, W. Makowski, M.C. Igualada López, J. Martínez Triguero and F. Rey, *J. Catal.*, 2014, **312**, 46-57.
- 12 K. Sadowska, A. Wach, Z. Olejniczak, P. Kuśtrowski and J. Datka, *Microporous Mesoporous Mater.*, 2013, **167**, 82-88.
- 13 K. Sadowska, K. Góra-Marek and J. Datka, *J. Phys. Chem. C*, 2013, **117**, 9237-9244.
- 14 K. Sadowska, K. Góra-Marek and J. Datka, *Vib. Spectrosc.*, 2012, **63**, 418-425.
- 15 S. Abelló, A. Bonilla and J. Pérez-Ramírez, *Appl. Catal. A*, 2009, **364**, 191-198.
- 16 Y. He, M. Liu, C. Dai, S. Xu, Y. Wei, Z. Liu and X. Guo, *Chin. J. Catal.*, 2013, **34**, 1148-1158.
- 17 J. Garcia-Martinez, M. Johnson, J. Valla, K. Li and J.Y. Ying, *Catal. Sci. Technol.*, 2012, **2**, 987-994.
- 18 V.V. Ordonsky, I.I. Ivanova, E.E. Knyazeva, V.V. Yuschenko and V.I. Zaikovskii, *J. Catal.*, 2012, **295**, 207-216.
- 19 W. Tjandra, J. Yao and K.C. Tam, *Langmuir*, 2006, **22**, 1493-1499.
- 20 J. Jung, C. Jo, F.M. Mota, J. Cho and R. Ryoo, *Appl. Catal. A*, 2015, **492**, 68-75.

- 21 D. Verboeckend, G. Vilé and J. Pérez-Ramírez, *Cryst. Growth Des.*, 2012, **12**, 3123-3132.
- 22 D. Verboeckend, M. Milina, S. Mitchell and J. Pérez-Ramírez, *Cryst. Growth Des.*, 2013, **13**, 5025-5035.
- 23 F. Thibault-Starzyk, I. Stan, S. Abelló, A. Bonilla, K. Thomas, C. Fernandez, J.-P. Gilson and J. Pérez-Ramírez, *J. Catal.*, 2009, **264**, 11-14.
- 24 N.S. Nesterenko, F. Thibault-Starzyk, V. Montouillout, V.V. Yushchenko, C. Fernandez, J.P. Gilson, F. Fajula and I.I. Ivanova, *Kinet. Catal.*, 2006, **47**, 40-48.
- 25 K. Góra-Marek, K. Tarach and M. Choi, *J. Phys. Chem. C*, 2014, **118**, 12266-12274.
- 26 K. Sadowska, K. Góra-Marek, M. Drozdek, P. Kuśtrowski, J. Datka, J. Martinez Triguero and F. Rey, *Microporous Mesoporous Mater.*, 2013, **168**, 195-205.
- 27 Y. Wang, Y. Sun, C. Lancelot, C. Lamonier, J.-C. Morin, B. Revel, L. Delevoye and A. Rives, *Microporous Mesoporous Mater.*, 2015, **206**, 42-51.
- 28 H. Liu, H. Wei, W. Xin, C. Song, S. Xie, Z. Liu, S. Liu and L. Xu, *J. Energy Chem.*, 2014, **23**, 617-624.
- 29 A. Széchenyi and F. Solymosi, *Catal. Lett.*, 2008, **127**, 13-19.
- 30 H. Liu, S. Liu, S. Xie, C. Song, W. Xin and L. Xu, *Catal. Lett.*, 2015, **145**, 1972-1983.
- 31 L. Zhang, H. Liu, X. Li, S. Xie, Y. Wang, W. Xin, S. Liu and L. Xu, *Fuel Process. Technol.*, 2010, **91**, 449-455.
- 32 I.I. Ivanova, I.A. Kasyanov, A.A. Maerle and V.I. Zaikovskii, *Microporous Mesoporous Mater.*, 2014, **189**, 163-172.
- 33 N. Gao, S. Xie, S. Liu, W. Xin, Y. Gao, X. Li, H. Wei, H. Liu and L. Xu, *Microporous Mesoporous Mater.*, 2015, **212**, 1-7.
- 34 Y. Lv, X. Qian, B. Tu and D. Zhao, *Catal. Today*, 2013, **204**, 2-7.
- 35 C. Fernandez, I. Stan, J.P. Gilson, K. Thomas, A. Vicente, A. Bonilla and J. Pérez-Ramírez, *Chem. Eur. J.*, 2010, **16**, 6224-6233.
- 36 O. Awayssa, N. Al-Yassir, A. Aitani and S. Al-Khattaf, *Appl. Catal. A*, 2014, **477**, 172-183.
- 37 B. Gil, L. Mokrzycki, B. Sulikowski, Z. Olejniczak and S. Walas, *Catal. Today*, 2010, **152**, 24-32.
- 38 K. Leng, Y. Wang, C. Hou, C. Lancelot, C. Lamonier, A. Rives and Y. Sun, *J. Catal.*, 2013, **306**, 100-108.
- 39 A. Bonilla, D. Baudouin and J. Pérez-Ramírez, *J. Catal.*, 2009, **265**, 170-180.
- 40 M. Milina, S. Mitchell, D. Cooke, P. Crivelli and J. Pérez-Ramírez, *Angew. Chem. Int. Ed. Engl.*, 2015, **54**, 1591-1594.
- 41 J.D. Na, G.Z. Liu, T.Y. Zhou, G.C. Ding, S.L. Hu and L. Wang, *Catal. Lett.*, 2013, **143**, 267-275.
- 42 I.I. Ivanova and E.E. Knyazeva, *Chem. Soc. Rev.*, 2013, **42**, 3671-3688.
- 43 J.C. Groen, L.A. Peffer, J.A. Moulijn and J. Pérez-Ramírez, *Chem. Eur. J.*, 2005, **11**, 4983-4994.
- 44 J.C. Groen, J.A. Moulijn and J. Pérez-Ramírez, *J. Mater. Chem.*, 2006, **16**, 2121-2131.
- 45 I. Grosse and K. Estel, *Colloid. Polym. Sci.*, 2000, **278**, 1000-1006.
- 46 L. Wang, Y. Wang, A. Wang, X. Li, F. Zhou and Y. Hu, *Microporous Mesoporous Mater.*, 2013, **180**, 242-249.
- 47 M.L. Gou, R. Wang, Q. Qiao and X. Yang, *Microporous Mesoporous Mater.*, 2015, **206**, 170-176.
- 48 T.C. Keller, J. Arras, S. Wershofen and J. Pérez-Ramírez, *ACS Catal.*, 2015, **5**, 734-743.
- 49 S. Mitchell, M. Milina, R. Verel, M. Hernandez-Rodriguez, A.B. Pinar, L.B. McCusker and J. Pérez-Ramírez, *Chem. Eur. J.*, 2015, **21**, 14156-14164.
- 50 H. Liu, H. Wei, W. Xin, S. Xie, Z. Liu, S. Liu and L. Xu, *Acta. Pet. Sin. (Pet. Process.)*, 2014, **30**, 115-120.
- 51 J. Jae, G.A. Tompsett, A.J. Foster, K.D. Hammond, S.M. Auerbach, R.F. Lobo and G.W. Huber, *J. Catal.*, 2011, **279**, 257-268.
- 52 J. Pérez-Ramírez, D. Verboeckend, A. Bonilla and S. Abello, *Adv. Funct. Mater.*, 2009, **19**, 3972-3979.
- 53 M.H.M. Ahmed, O. Muraza, A.M. Al Amer, Y. Sugiura and N. Nishiyama, *Microporous Mesoporous Mater.*, 2015, **207**, 9-16.
- 54 T.S. Zhao, T. Takemoto and N. Tsubaki, *Catal. Commun.*, 2006, **7**, 647-650.
- 55 A. Galadima and O. Muraza, *Microporous Mesoporous Mater.*, 2015, **213**, 169-180.
- 56 H. Wang and W. Xin, *Catal. Lett.*, 2001, **76**, 225-229.
- 57 N. Gao, S. Xie, S. Liu, J. An, X. Zhu, L. Hu, H. Wei, X. Li and L. Xu, *Catal. Lett.*, 2014, **144**, 1296-1304.
- 58 D. Verboeckend and J. Pérez-Ramírez, *ChemSusChem*, 2014, **7**, 753-764.



Catalysis Science & Technology

ARTICLE

The composite effects of NaOH and CTAB regulated the porosity and acidity of ZSM-11 samples, which affected the reaction stability.

